Earthquakes and Structures, *Vol. 16, No. 3 (2019) 329-348*
DOI: https://doi.org/10.12989/eas.2019.16.3.329

Effect of masonry infilled panels on the seismic performance of a R/C frames

Hassan Aknouche*[1], Abdelhalim Airouche[a] and Hakim Bechtoula[b]

National Earthquake Engineering Research Centre, C.G.S., Rue Kaddour RAHIM, BP 252 Hussein Dey, Alger, Algeria

(Received November 1, 2018, Revised January 27, 2019, Accepted February 1, 2019)

Abstract. The main objective of this experimental research was to investigate the Seismic performance of reinforced concrete frames infilled with perforated clay brick masonry wall of a type commonly used in Algeria. Four one story-one bay reinforced concrete infilled frames of half scale of an existing building were tested at the National Earthquake Engineering Research Center Laboratory, CGS, Algeria. The experiments were carried out under a combined constant vertical and reversed cyclic lateral loading simulating seismic action. This experimental program was performed in order to evaluate the effect and the contribution of the infill masonry wall on the lateral stiffness, strength, ductility and failure mode of the reinforced concrete frames. Numerical models were developed and calibrated using the experimental results to match the load-drift envelope curve of the considered specimens. These models were used as a bench mark to assess the effect of normalized axial load on the seismic performance of the RC frames with and without masonry panels. The main experimental and analytical results are presented in this paper.

Keywords: masonry infill panel; seismic performance; strength; stiffness; ductility; failure mode

1. Introduction

Many existing and new buildings in Algeria, made of reinforced concrete (RC) frames are usually filled in by perforated clay brick masonry wall, due to the high fire resisting capacity and the economical and relatively excellent thermal and sound insulator. Brick wall is considered as the most widely accepted infill material in the context of Algeria and all the world. The framed-masonry structure serves both architectural and structural demands efficiently.

Unreinforced masonry infill panels are used as partitions in RC frames and typically considered as non-structural elements in the Algerian seismic code, RPA99/2003 (MHUV 2003), and their role in the structural response has often been underestimated or completely neglected in design practice. The Algerian seismic design code, as many other codes, neglects the effect of masonry panels and therefore, the structure is designed as a bare frame.

However, observations from recent earthquakes, Boumerdes 2003 (Masanori and Kheir-Eddine 2004) have shown that under seismic excitation, the structural interaction between columns and infill walls can significantly affect the structural behavior and alter the load resisting mechanism and failure pattern of the RC frame.

Their interaction is recognized in the global behaviour of RC frame by a number of significant experimental tests and analytical research performed in last 50 years (Brokken and Bertero 1981, Lotfi and Shing 1994, Flanagan and Bennett 1999, Pinto *et al.* 2000, Calvi and Bolognini 2001, Ghassan

2004, Kakaletsis and Karayannis 2007, Stylianidis 2012, Misir *et al.* 2012, Maidiawati 2013, Tsung-Chih and Shyh-Jian 2015, Alessandro and Camillo 2015, Ivan *et al.* 2016, Hamid and Kadir 2016, Aksel *et al*. 2016, Teguh 2017, Yasushi *et al.* 2017).

A review of the literature on infilled-frames shows that two different research approaches can be identified, one aiming to strengthen the infill, by various methods in order to improve the resistance and monolithic behaviour of the frame and infill (Ali *et al.* 2015), the other to limit the infill frame interaction by certain provisions or devices in order to reduce infill damage and its detrimental effects to the frame. Reducing the infill strength and stiffness or isolating the infill panel masonry from the column is proposed in many recent research (Preti *et al*. 2012, Gautam and Solomon 2014, Ozkaynak *et al.* 2014, Fabio 2015, Jarun *et al.* 2017, Hanhui 2017, Shabdin *et al.* 2018, Terry *et al.* 2018).

The main objective of this experimental research was to investigate the seismic performance of reinforced concrete frames infilled with perforated clay brick masonry wall of a type commonly used in Algeria. Four one story-one bay reinforced concrete infilled frames of half scale of an existing building were tested at the National Earthquake Engineering Research Center Laboratory, CGS, Algeria. The experiments were carried out under a combined constant vertical and reversed cyclic lateral loading simulating seismic action. This experimental program was performed in order to evaluate the effect and the contribution of the infill masonry wall on the lateral stiffness, strength, ductility and failure mode of the reinforced concrete frames.

∗Corresponding author, Ph.D.
E-mail: haknouche_70@yahoo.fr
[a]Ph.D.
[b]Professor

http://www.techno-press.com/journals/eas&subpage=7 ISSN: 2092-7614 (Print), 2092-7622 (Online)

Fig. 1 External panel with masonry infill

Fig. 2 Collapse of external infill walls of the first story

Fig. 3 Collapse of external infill walls of higher stories

Fig. 4 General view of 2-story damaged masonry stone building

2. Behavior of RC frame with masonry infill

Reinforced concrete frame buildings are the most popular in Algeria, particularly for buildings up to 10 stories. Perforated clay brick masonry infill walls with dimensions of 300×200×100 mm in length, height and width respectively; are often used to separate the interior building area. The exterior panels are executed with two infill walls using hollow clay bricks. For high-rise buildings, more than 15 stories, reinforced concrete shear wall structures are used. In some cases, mixed structures, frames and shear walls, are used. External panels are either executed with masonry infill, shown in Fig. 1 or prefabricated reinforced concrete panels.

The Algerian seismic design code, as many other codes, neglects the effect of masonry panels and therefore, the structure is designed as a bare frame. The masonry infill panel is considered as non-structural components.

During the May 21st, 2003 Zemmouri earthquake, reinforced concrete shear wall structures suffered slight to no damage. For the majority of the damaged RC frame buildings, masonry of the first floor broke out and plastic hinges were developed near the columns joints, leading to soft story and in several cases to floor mechanisms.

Observed damage to the RC frame buildings after the Zemmouri earthquake can be partly attributed to ignorance of the interaction between the frame and masonry in design practice and partly to the low quality of construction. In Algeria, generally, external masonry panels are constituted of 2 hollow brick walls that are weakly connected to each other and not rigidly connected to frames, at all. Example of the out of plane collapse is shown in Fig. 2. For some old reinforced concrete buildings, the external masonry wall is continuous from the first story to the last one without any ties, which make it very vulnerable to horizontal shakings (Ousalem and Bechtoula 2003). A case of 15-story reinforced concrete frame building can be seen in Fig. 3.

Such structures are at least 50 years old and were using the most popular construction type at that time before the introduction of the dual reinforced concrete type. Another construction system consists of using bearing stone walls of 40 to 60 cm thick. The floors are made in some cases of wood or in other cases of brick arches supported by steel beams, filled with earth materials. Stone masonry buildings within 60 km from the epicenter suffered a lot from the earthquake (Ousalem and Bechtoula 2003). Typical damages, like diagonal shear of bearing stone walls, lack of ties near openings, weak connection between bearing walls and slabs, and out of plane failure of some walls, are shown through Fig. 4.

3. Prototype structure

The prototype structure chosen in this study is a typical 4-storey residential, reinforced concrete frame building in urban areas in Algeria, which was designed before the Algerian seismic code, RPA99/2003 (MHUV 2003), according to functionality of the building and seismic Zone III, corresponding to the design peak ground acceleration of 0.15g. The selected building is one among 21 others representing a construction program of 70 apartments located at Zeralda, east of Algiers. The construction started 5 months before the 6.8MW, 2003, Boumerdes Earthquake.

The design strengths of concrete is 25 MPa, and 400 MPa for longitudinal and transversal reinforcement. The model represents the lower part of the real building that was scaled down to one-half scale.

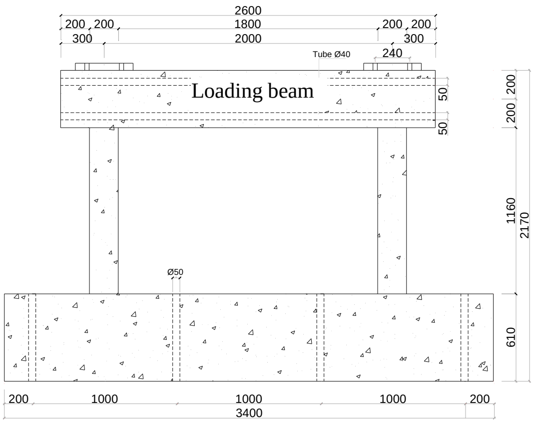

Fig. 5 Dimensions of the frames

Table 1 Steel reinforcement in columns

Column	Reinforcement	A_s (cm^2)	Ratio
Longitudinal reinforcement	8T8	4.02	1%
Transversal reinforcement Critical Zone L=380 mm	4ϕ6@35 mm	1.70	1.62%
Transversal reinforcement Non-Critical Zone e=400 mm	4ϕ6@50 mm	1.70	1.13%

4. Test specimens

The experimental program consists of four specimens, one-bay and one-storey RC frame specimens, two bare frames without masonry infill wall and two with masonry infill wall. Dimensions and the amount of the steel reinforcements of the RC frame were identical for all specimens. The cross-section of the loading beam and the columns were 300×400 mm, and 200×00 mm, respectively. Dimensions of the tested frames are shown in Fig. 5.

In the critical zones, located at both ends of the columns, stirrups of ϕ6 were set every 35 mm, outside these zones the spacing was to 50 mm. Table 1 summarizes the amount of the steel reinforcement in the columns.

Longitudinal reinforcement bars were of type FeE400 with a yield strength, f_y=400 N/mm^2, an ultimate strength f_u=480 N/mm^2 and a Young modulus of E=206957 N/mm^2. The yield strength of transversal reinforcement of columns (FeE215) ϕ6 steel bar is 215 MPa, ultimate strength is 330 MPa, and Young's Modulus is 200 GPa.

Concrete cylinder of 320 mm 160 mm in height and diameter, respectively, for different batches, were made during the specimen casting and kept under the same environmental conditions. The compressive strength of the first batch of cylinder was tested 28 days after the specimens were cast, and the remaining batches of the cylinders were tested on the test day of the infilled frame specimens. The average 28-day cylinder strength is 25 MPa. It is noted that the mix is a normal mix which was prepared with sands, gravels, and cement.

The four specimens were constructed at the CGS laboratory. Ordinary workmanship was intentionally employed in specimen construction. Fig. 6, shows the steel gages of the foundations and the reinforcement of the columns. The masonry infill wall was made with perforated-clay bricks and cement mortar. The masonry infill panels were built after the RC frame was made and hardened.

Fig. 6 Construction of the test specimens at CGS laboratory

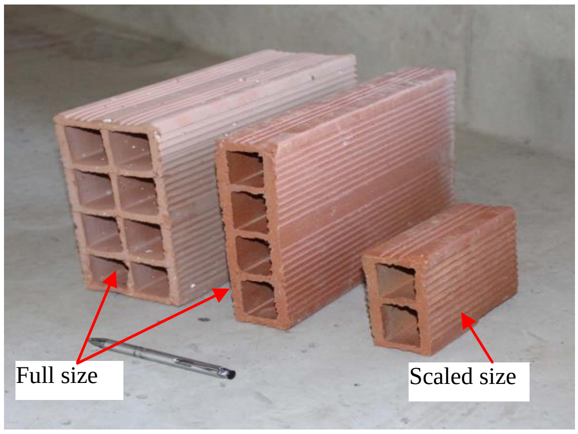

Fig. 7 Full and scaled size brick

To reproduce the exact number of mortar joints in the masonry wall, the appropriate size of bricks was important issue in the study. Small brick produced by the factory has a little strength and was more burnt than the full scale brick because the size of the brick affects the firing process (Egermann 1991). Therefore, in this work, the cutting method suggested by other researchers was employed (Hughes and Kitching 2000). A clay brick with an approximate size of 300×200×100 mm in length, height and width, respectively, was used in the real building. The scaled bricks were obtained by cutting bricks of 300×200×50 mm, to get two small pieces with an approximate size of 150×100×50 mm, as shown in Fig. 7.

Table 2 summarizes the perforated ratio and the weight of the full size brick and the scaled brick.

The mix proportion of mortar constituents considered in this work is the most used on the construction works of masonry in Algeria. Cement to sand ratio of cement mortar was 1:3 by weight. The mortar strength was found to be 14.5 N/mm^2. The obtained compressive strengths of masonry brick was 2.8 N/mm^2 and 14.5 N/mm^2 for mortar used in the masonry wall panels. The compressive strength

Table 2 Perforated ratio and the weight of the brick masonry

Dimensions of Brick (mm)	Perforated Ratio (%)	Weight (Kg)
300×200×100 (Full size)	62	4.2
300×200×50 (Full size)	53	2.4
150×100×50 (scaled size 1/2)	52	0.6

Table 3 Test variable

Specimen	Type	Loading
1	Bare frame	Pushover
2	Bare frame	Reversed cyclic
3	Frame with full panel	Reversed cyclic
4	Frame with opened panel	Reversed cyclic

Fig. 8 RC bare frame with a full infill masonry panel

of the brick depends strongly on the production process.

Prism test and shear bond test are desirables to characterize the material properties of the masonry. These tests are a better representation of the actual masonry construction, it includes the effects of the properties of the constituents of the masonry and the quality of workmanship. However, in the absence of the prism test and shear bond test, mathematical models proposed by local recommendations (DTRC2-45 2005) were used. For example, to predict the strength of masonry prism, f_p, the flowing Eq. (1) can be used

$$f_p = 0.55\sqrt[3]{f_m f_b^2} \tag{1}$$

Fig. 9 RC bare frame with a opening centric infill masonry panel

Where f_m and f_b are the compressive strength of the brick masonry and the mortar, respectively. The strength of masonry prism was 4.6 N/mm^2.

The brick masonry was installed between the two columns with two configurations. One of these frames was with a full infill masonry wall and another frame with a centric window opening having dimensions of 500 mm×500 mm, as illustrated in Figs. 8-9. Infill masonry panel was connected to the frame by mortar only.

The test variables of this research program are summarized in Table 3.

5. Test setup and Instrumentation

The reaction wall, strong floor, and the loading frame were used to carry out this testing program at C.G.S laboratory, as illustrated in Figs. 10(a)-(b).

The specimens were tested under combined constant vertical and reversed cyclic lateral loading simulating seismic action. The vertical load of approximately 100 kN, that simulated loading from the upper stories (four stories), was exerted on each RC column by means of two MTS servo-hydraulic actuators of 500 kN capacity.

During the test, those hydraulic actuators were manually controlled to maintain a constant vertical load within 1% tolerance.

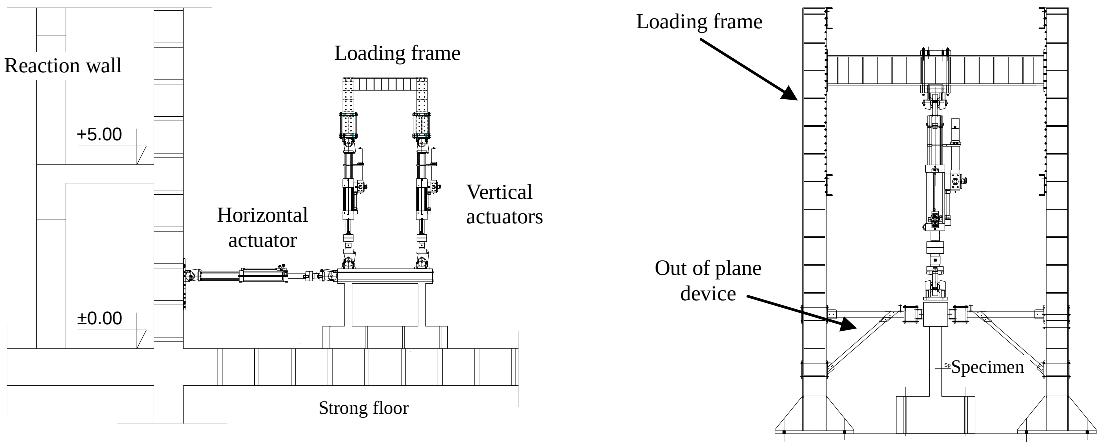

(a) Longitudinal view (b) Transversal view

Fig. 10 Test setup

Table 4 Drift angle

Rd	Drift (%)	Displacement (mm)	Loading Rate for 1mm
1/1000	0.1	1.36	10 Sec
1/500	0.2	2.72	
1/250	0.4	5.44	
1/150	0.67	9.112	
1/100	1	13.6	
1/67	1.5	20.4	5 Sec
1/50	2	27.2	
1/33	3	40.8	
1/25	4	54.4	

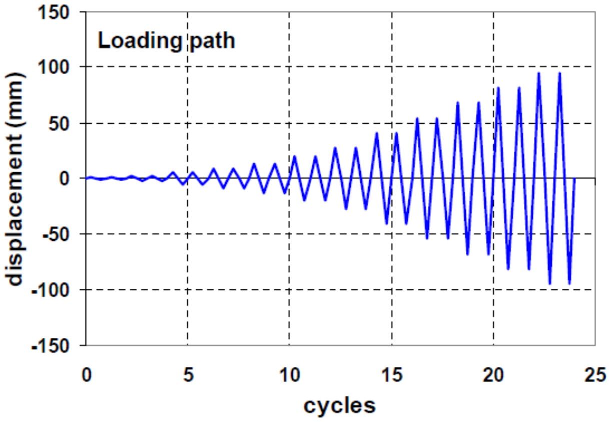

Fig. 11 Cycle loading pattern

The lateral load was applied to specimens through the loading beam, using one MTS-Servo hydraulic actuator. The lateral reversed cyclic loading was controlled by the top frame displacement.

Drift angle (Rd), defined as the ratio of lateral displacement to column height, was used to control the incremental loading. The loading path, displacement control, were defined and introduced before starting the test. In our case, the loading speed was not constant during the execution of the test, but it varied from 1 mm/10 sec at the beginning of the loading to 1 mm/5 sec after the drift displacement reach the value of 1%. The loading path and the loading rate were set as shown in Table 4. Time history of the lateral loading is shown in Fig. 11.

A global view of the loading frame with the actuators and the first bare frame is shown in Figs. 10(a)-(b). During testing, damage progress such as, masonry crushing, crack developments in masonry and concrete, crack pattern were visually observed and registered. All specimens were tested in the same manner.

Specimens were instrumented with thirteen (13) linear variable displacement transducer LVDTs to measure displacements at different locations of the specimens. Two LVDT's were used to control the lateral drift, The average shear displacement of the infill wall was measured by two diagonal LVDT's (LVDT N°7 et N°8). Eight LVDT's were located at the ends of the columns to measure the deformation at plastic hinge regions, and two LVDT's were used to measure the slip between the strong floor and the foundation and the uplift displacement of the frame.

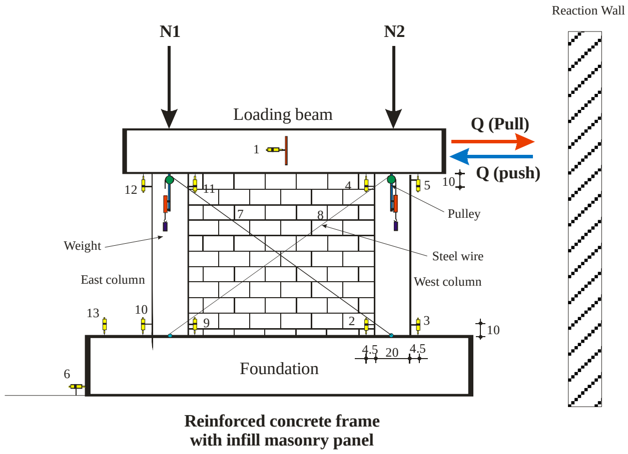

Fig. 12 Frame instrumentation

Due to the limited acquisition channels of our system, only eight (08) strain gauges were set on the reinforcements of the west column, two (02) strain gages on the stirrups (external and internal hoops) and two (02) strain gages on the vertical bars (external and internal bars).

The strain gauges were set at two (02) different levels located at 65 mm from the top and the bottom of the west column. During the whole test process, displacement and steel strains were recorded using MTS, FlexTest for LVDT's and DynaticWave for strain gauge. Location of these LVDTs on the frame is shown in Fig. 12.

6. Experimental results

This experimental program allowed us to investigates the seismic performance of masonry infilled frames, through a comparison, between specimens, of the hysteretic behavior, ductility factor, strength deterioration, stiffness degradation, variation of the equivalent viscous damping ratio, energy dissipation capacity, deformation and failures modes.

6.1 Hysteretic behaviour

The collected data provides us information regarding the response of the frame to the cyclic loading. The hysteresis loops shown below illustrate the lateral load vs. displacement response for specimens 1 and 2 shown in Figs. 13(a)-(b), and specimens 3 and 4 shown in Figs. 14(a)-(b). Stable hysteretic loops were observed during the entire loading path.

From Fig. 13(a) some fluctuation can be seen on the force drift curve. These fluctuations are due to the difficulty to control the vertical load applied to the columns around 2% drift. We should note that, during the test, the actuators (verticals and horizontals) were set to the desired loading path using the automatically control, force and displacement control, respectively. Fig. 15, illustrates the envelope curves of the four tested specimens.

Table 5 shows a comparison between the four specimens in terms of peak loads and the corresponding drifts. For specimen 3, frame with masonry infill panel, the

Table 5 Peak load ratios and corresponding drifts for the four specimens

Specimen	Direction	Peak load (KN)	Corresponding drift (%)	Ratio for the same specimen		Ratio between specimens and specimen 1	
				Load	Drift	Load	Drift
1	(+) Push	78,66	1,17			1,00	1,00
2	(+) Push	85,60	1,31	1.15	0.95	1,09	1,12
	(-) Pull	74,37	1,39			0,95	1,19
3	(+) Push	200,67	0,21	0,97	0,57	2,55	0,18
	(-) Pull	206,36	0,37			2,62	0,31
4	(+) Push	131,74	0,30	1,12	0,90	1,67	0,25
	(-) Pull	117,99	0,33			1,50	0,28

Table 6 Peak loads ratios and corresponding drifts between the first and the second cycles

Specimen	Cycle	Peak load (KN)		Ratio peak load 2nd/1st (%)		Drift (%)	
		Push	Pull	Push	Pull	Push	Pull
1	Pushover	78,66				1.167	
2	1st	85,60	-74,37	0,90	0,94	1.310	-1.386
	2nd	77,27	-70,09			1.449	-1.405
3	1st	200,67	-206,36	0,65	0,91	0.207	-0.365
	2nd	129,58	-187,02			0.292	-0.286
4	1st	131,74	-117,99	0,85	0,89	0.296	-0.329
	2nd	112,15	-105,45			0.315	-0.341

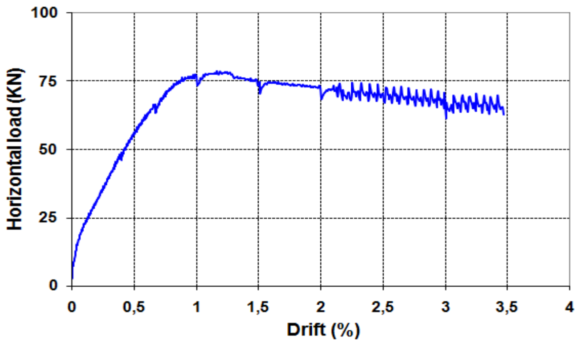

(a) Specimen 1

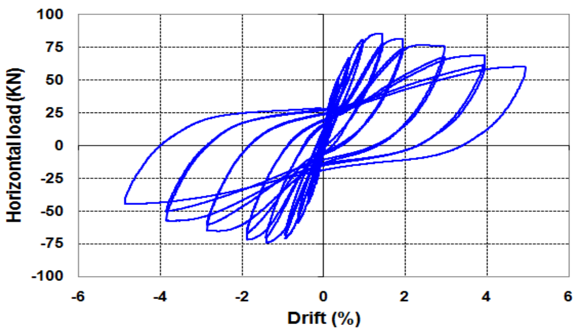

(b) Specimen 2

Fig. 13 Load-drift relationship (bare frames)

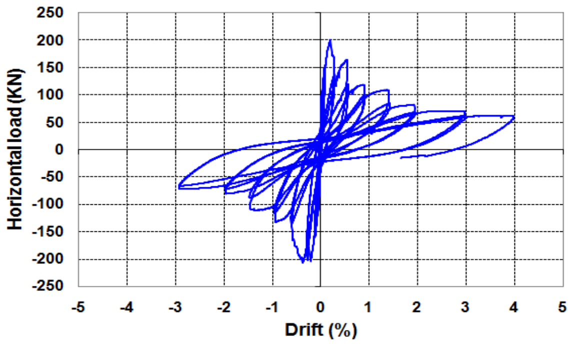

(a) Specimen 3

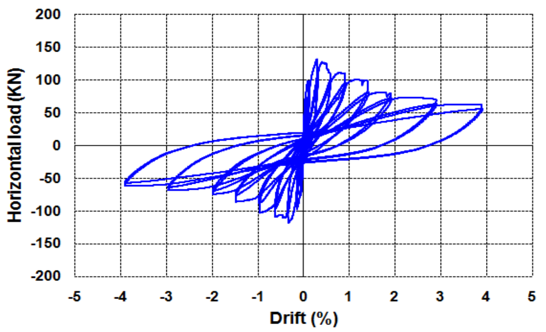

(b) Specimen 4

Fig. 14 Load-drift relationship (frames with masonry)

peak load was increased to 2.55 times in the push side and 2.62 times in the pull side, while compared to the peak load reached for the bare frame, specimen 1. These values were, respectively, 1.67 and 1.50 for specimen 4 with an centric opening infill masonry panel.

As shown in Table 6, and while comparing the drifts to the drift reached for the specimen 1, the drift of specimen 3 was decreased to 0.18 times in the push side and 0.31 times in the pull side. These values were, respectively, 0.25 and 0.28 for specimen 4.

From Fig. 15, it is clear that the envelope curve of specimen 2, tested under reversed cyclic loading, fits very well the envelope curve of specimen 1, tested under monotonic loading (pushover). Also, it can be seen that the envelopes curves of specimens 3 and 4 matches that of specimen 2 after ±2% drifts.

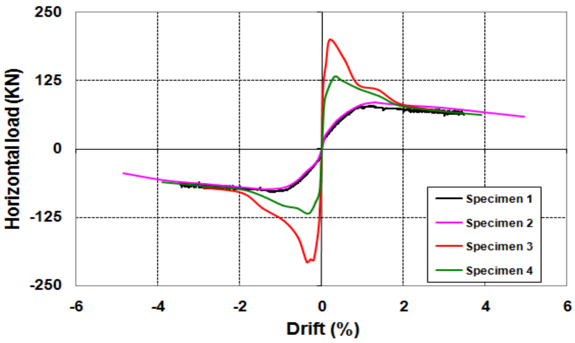

Fig. 15 Load-drift envelope curves

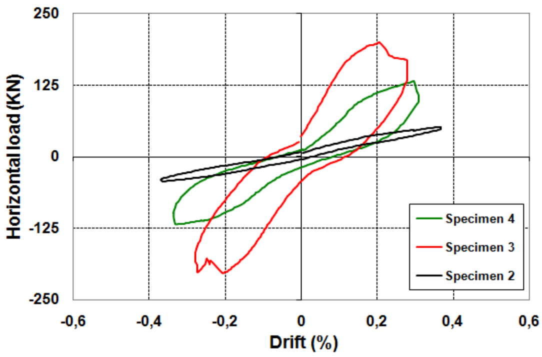

(a) *R*=1/100

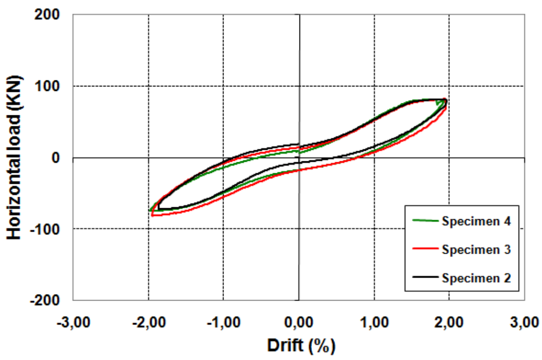

(b) *R*=1/50

Fig. 16 Variation of the hysteretic loop shapes with respect to the drift, for specimens 2, 3 and 4

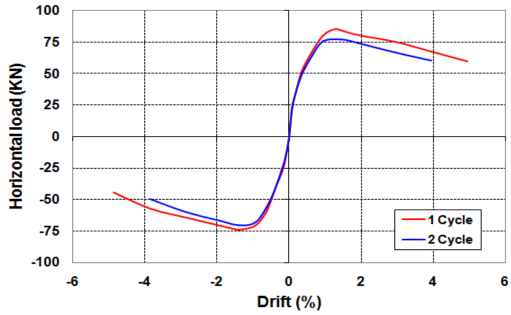

(a) Specimen 2

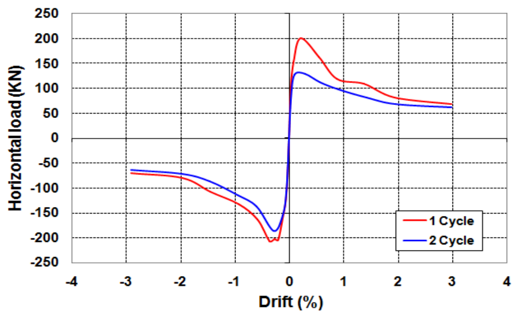

(b) Specimen 3

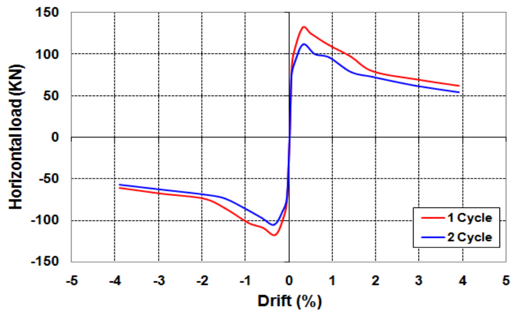

(c) Specimen 4

Fig. 17 Comparison between the first and the second envelope curves

This is because at that time the masonry wall was completely damaged and it remains only the reinforced concrete frame. This fact can be also seen in Figs. 16(a)-(b) while comparing the hysteretic loops of the three specimens at different drifts (*R*=1/100 and *R*=1/50).

A big drop was observed in the peak load between the first and the second loading cycles in the push side for specimen 3 and 4 as illustrated in Figs. 17(b)-(c). This drop was 35% for specimen 3, due mainly to the damage of the brick masonry and 17% for specimen 4. For the pull side, around 10% drop was observed as shown in Table 6.

6.2 Displacement and ductility factor

6.2.1 Ductility factor

Ductility is the capability of a structural element or building to distort and yield without collapsing. During an earthquake, the ductility allows the structure to dissipate large quantity of energy even after the local yielding of members. There are number of definitions of ductility factor, all of which represent the ratio of some property at failure to that property at yielding. In this manuscript two calculation technique were used to calculate the displacement ductility. The first one (1), may be specified as the ratio of the maximum displacement to the displacement at yield point. The yielding displacements were those corresponding to the first yielding of the longitudinal reinforcements. The ultimate displacement is defined as the displacement corresponding to the peak load reduced of 20% of its maximum value in the push and pull sides.

The second one (2), is defined as the ratio of the average of the push and pull ductility's computed separately in which the yielding displacement was the average of the yielding displacements in push and pull sides and the maximum displacements corresponding to 20% drop of the peaks load in the push and pull sides. Figs. 18(a)-(b) illustrate the variation of the computed ductility using the

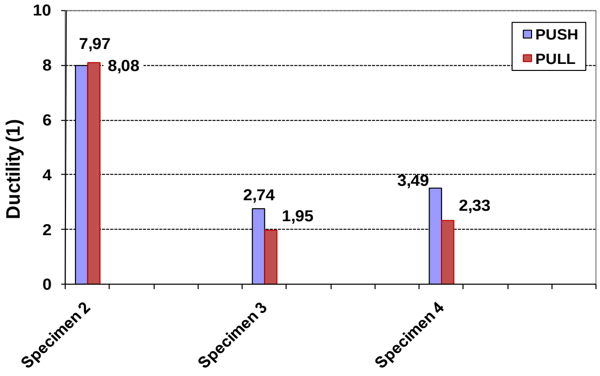

(a) Method (1)

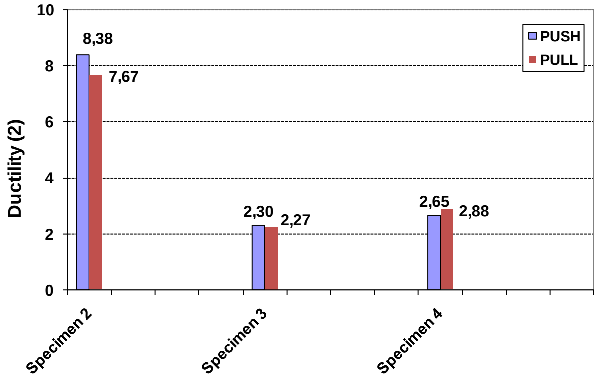

(b) Method (2)

Fig. 18 Ductility factor

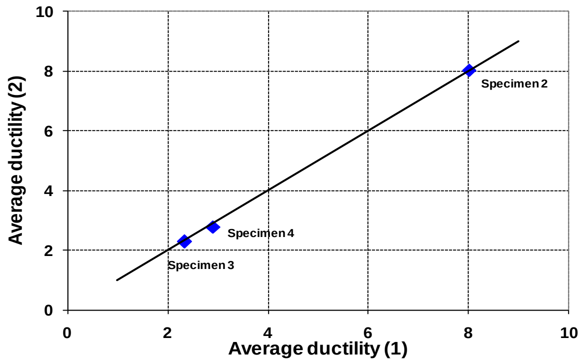

Fig. 19 Effect of infill masonry wall on the ductility factor

two methods, described above, in push and pull side.

Under the cyclic loading, the average yield displacement (+6.25 mm) of bare frame is larger than that of the infilled frame (+3.41 mm) and the centric opening infill frame (+5.69 mm). It can be seen from Figs. 18(a)-(b), that the bare frame (specimen 2) have a larger ductility in push and pull side. The average ductility of the bare frame is about 3 times of the centric opening infill masonry wall frame and 3.5 times of the full infill masonry wall frame. As illustrated in Fig. 19, the two techniques used to calculate the ductility factors gave nearly the same ductility for the three specimens; obtained results are lying on the same line of 45°.

6.2.2 Flexural and shear deformation

Flexural and shear contribution to the frame top displacement were calculated using the following equations

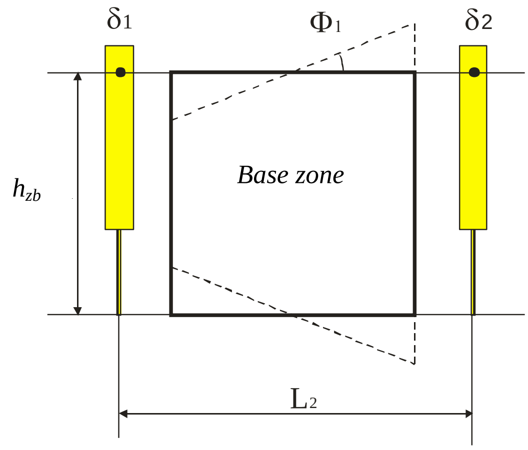

Fig. 20 Curvature for base zone

$$\Delta = \Delta_f + \Delta_s + \Delta_R \tag{2}$$

Where :

Δ is the frame top displacement,

Δ_f is the flexure contribution,

Δ_s is the shear contribution,

Δ_r the rocking contribution.

The flexural contribution to top displacement, for the base zone for example, were computed as follows (Bechtoula 2002)

$$\Delta_{fzb} = \phi_{zb} h_{zb} (l_b + h_{zb}/2) \tag{3}$$

Where

Δ_{fzb} is the flexural contribution to top displacement,

h_{zb} is the height of the considered zone,

l_b is the distance between the top zone and the column loading point,

ϕ_{zb} is the curvature for the considered zone.

The curvature ϕ_{zb} is calculated for the base zone as follows

$$\phi_{zb} = \frac{\delta_2 - \delta_1}{L_2 h_{zb}} \tag{4}$$

Where:

δ_1 and δ_2 are respectively the displacement recorded by LVDTs installed at the base of the considered zone on the two faces of the column, see Fig. 20.

L_2 the distance between the two LVDT1 and LVDT2, as shown in Fig. 20

The shear contribution is calculated using the flowing equations

$$\Delta_s = \gamma h \tag{5}$$

With h is the height of the frame and γ is the shear distortion given by Eq. (6)

$$\gamma = \frac{\sqrt{h^2 + l^2}}{2hl} (\delta_8 - \delta_7) \tag{6}$$

In Eq. (6), l is the distance between the two columns, h is the distance between the base of the column to mid height

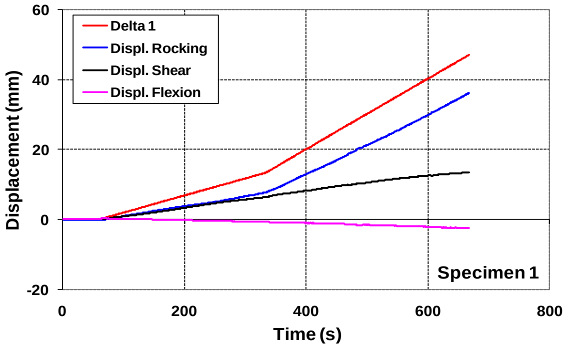

(a) Specimen 1

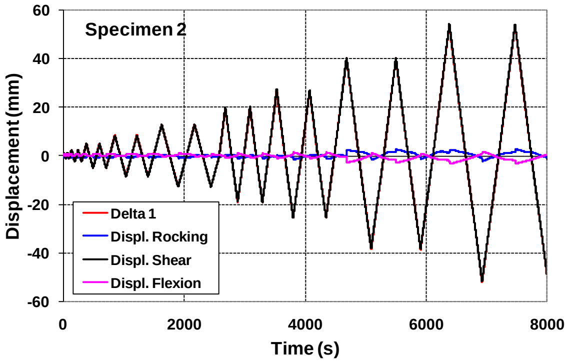

(b) Specimen 2

Fig. 21 Flexural and shear contribution to the top frame displacement (bare frame)

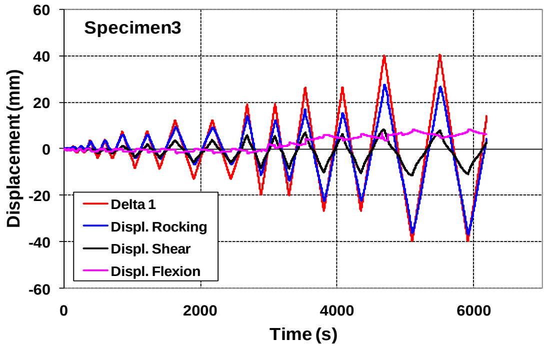

(a) Specimen 3

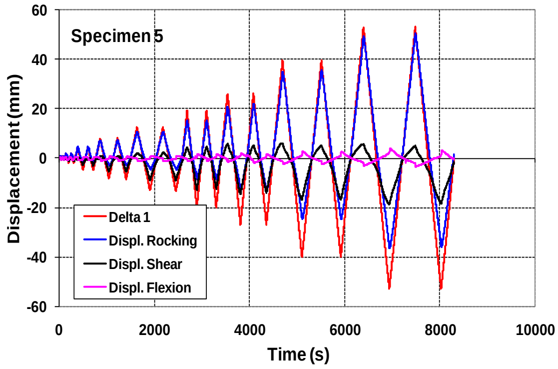

(b) Specimen 4

Fig. 22 Flexural and shear contribution to the top displacement (frame with masonry)

of the loading beam, and δ_7 and δ_8 are, respectively, the diagonal displacement recorded by LVDT 7 and 8 shown in Fig. 12.

Figs. 21(a)-(b) and Figs. 22(a)-(b) shows the rocking, shear and the flexural contribution to the top frame displacement, Delta 1. As found for all specimens, the flexural contribution is negligible compared to the rocking and shear contribution. For specimen 2, the shear contribution is bigger than that of specimen 1.

Rocking deformation was the dominated part that contributed to the top displacement for the four tested specimens. This fact was mainly due to two raisons:

- We tested only one story without any real beam. Hence, the beam column connection is not well represented since in our case we have a loading beam that is very rigid compared to the column. By consequence, damage will be concentrated only on columns.
- In Algeria, we still using a very old construction method that consists to construct the vertical elements (columns and shear walls) of the structure after that to construct the floor (beams and slab). This method creates two "cold joints" between the floor and the bottom of the columns and the second between the top columns and the beams.

During a seismic event, and under a cyclic loading, these cold joints start to open and create a sway mechanism. This phenomenon was well observed during our testing program especially for specimen 1 and 2, bare frames, as illustrated in Fig. 23.

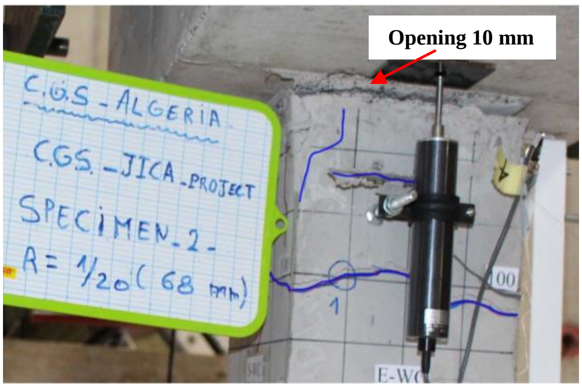

Fig. 23 Opening of 10 mm at top column-loading beam connection, 5% drift (specimen 2)

6.3 Strength deterioration and stiffness degradation

The initial stiffness of all specimens was obtained from the initial tangent modulus of the slopes of the capacity curves. Another type of stiffness can be derived from the hysteresis loops, which is called peak to peak stiffness. The slope of the line linking the positive and negative cycle is derived and compared within the same specimen at different displacement level to determine the stiffness degradation while damage progress in the specimen. Fig. 24 shows the shapes of the envelope curves for the first cycles at each drift of the loading path for the three specimens under cyclic loading. Specimen 2 demonstrate a fat loops compared to specimens 3 and 4. In the same time, it can be

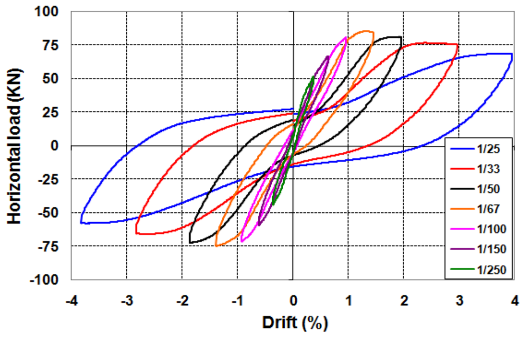

(a) Specimen 2

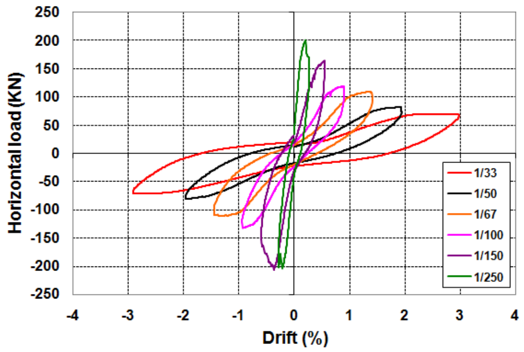

(b) Specimen 3

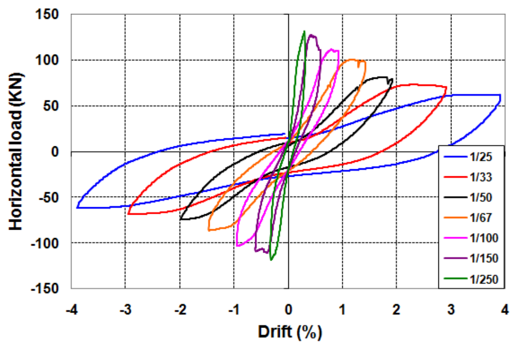

(c) Specimen 4

Fig. 24 Variation of the hysteretic loop shapes with respect to the drift

seen that the stiffness degradation of specimen 2 is less pronounced than that observed for specimens 3 and 4.

To strengthen this remarks, stiffness degradation was computed at each drift, for each specimen, and compared to the initial stiffness K_0, see Table 7 and Fig. 25.

Insertion of the masonry panel, compared to the bare frame, generates an increase of the initial rigidity of the order of 11.5 and 4.85 for the infill masonry and centric opening masonry wall, respectively, in the push side. These values were 13.15 and 6.72 in the pull side.

It can be seen from the different values of initial stiffness, shown in the Table 7, how the infill masonry panel influence the stiffness of the system. The bare frame is the specimen with the weaker initial stiffness, but with the largest ductility.

From Fig. 25, it can be seen that the stiffness degradation was significant after the maximum peak was reached and loss of stiffness tends asymptotically towards

Table 7 Initial stiffness K_0 (kN/m)

Direction	Specimen 2	Specimen 3	Specimen 4
Push side	200.94	2546.42	1070.55
Pull side	148.51	1953.24	998.52

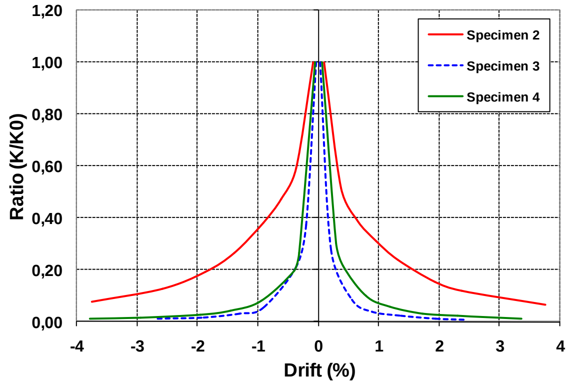

Fig. 25 Stiffness degradation

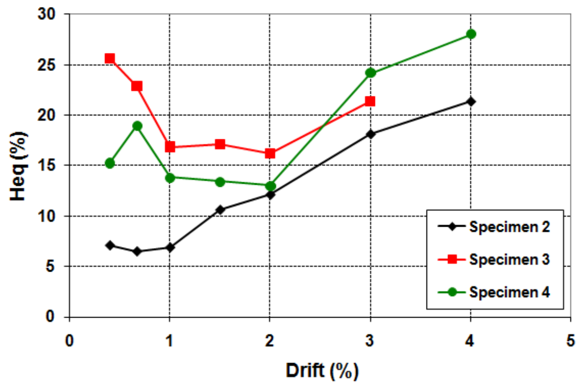

Fig. 26 Stiffness degradation

the bare frame at higher drifts. Stiffness degradation was more significant for specimen without opening than for specimen with opening. It can be concluded that the presence of infill masonry panel, even with opening, improves the initial stiffness of the frame compared to that of the bare frame. This stiffness must be taken into account during the design of the structure.

6.4 Variation of the equivalent viscous damping ratio

Variation of the equivalent viscous damping factor was computed using the first cycle loops at each of the imposed drift angle (Shibata and Zosen 1976). The equivalent viscous damping, H_{eq}, was computed using the following expression, Eq. (7).

$$H_{eq} = \frac{1}{4\pi}\frac{E_H}{E_{so}} \tag{7}$$

Where, E_H is the area enclosed in the hysteresis loop. E_{so} is the equivalent potential energy. Variations of the equivalent viscous damping for specimens 2, 3 and 4 are shown in Fig. 26.

Variation of the equivalent viscous damping was nearly

Table 8 Total energy dissipated (kN m)

Dissipation energy	Specimen 2	Specimen 3	Specimen 4
E (Total)	1027	1691	1341

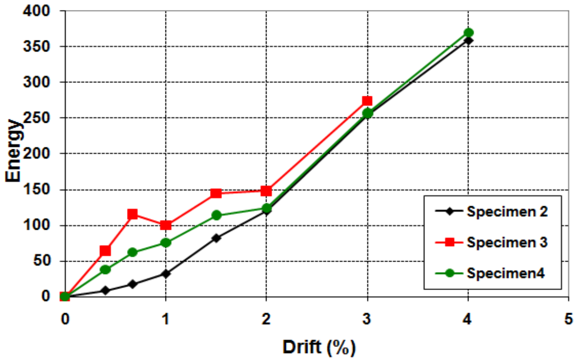

Fig. 27 Energy dissipation at each drift for all specimens

linear for specimen 2. A constant equivalent viscous damping was observed for specimen 3 and 4 between 1% and 2% drift. After 2% drift, specimens 3 and 4 show nearly the same slope on the H_{eq} drift curves.

This state indicates that only frame remains, after severe damage to the infill masonry panel for specimens 3 and 4.

6.5 Energy dissipation capacity

The energy dissipation capacity is one of the important parameter in the analysis of the behavior of the structure during an earthquake. Table 8 shows the total amount of the energy dissipated during the loading for the three specimens. Energy dissipated by specimen 3 was 126% and 164% higher than that dissipated by specimen 4 and specimen 2, respectively.

Fig. 27 shows a comparison of the dissipated energy of the three specimens at each drift. As clearly shown before, the upper bound is represented by specimen 3 while specimen 2 represents the lower bound. A variation of the energy dissipation for all specimens was observed between 0% and 2% drift. After 2% drift, specimens 3 and 4 show nearly the same slope on the dissipation energy drift curves as specimen 2. This state indicates that only frame remains, after the severe damage to the masonry infill panels for specimens 3 and 4.

6.6 Deformation at plastic hinge zones

Before casting of concrete, strain gauges were installed on the longitudinal reinforcement bars and on the stirrups. The strains gauges were located mainly near the critical zones, where the stress is supposed to be the maximum. The strain gauges were set at two (02) different levels located at 65 mm from the top and the bottom of the west column. We have to note that the yielding strain of the steel reinforcement is 0.002 (2000 MicroStrain).

Analysis of the collect strain gauge data showed that the main longitudinal reinforcement yielded either at the top or at the bottom of the column. For the transversal reinforcement no yielding was observed neither for the

Table 9 Strain gauge data

Longitudinal reinforcement	Strain ($\mu\varepsilon$)	Drift (%)	Yield displacement (mm)
Specimen 1	2000		
Specimen 2	2016	0.48	6.57
Specimen 3	2066	0.21	2.86
Specimen 4	2020	0.32	4.33

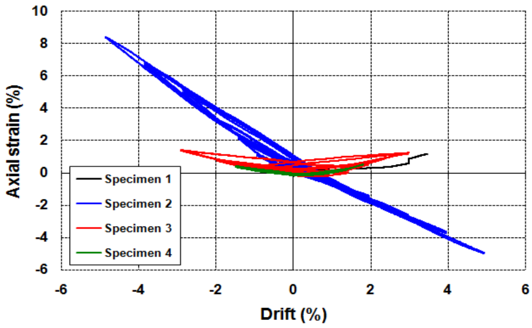

(a) Bottom

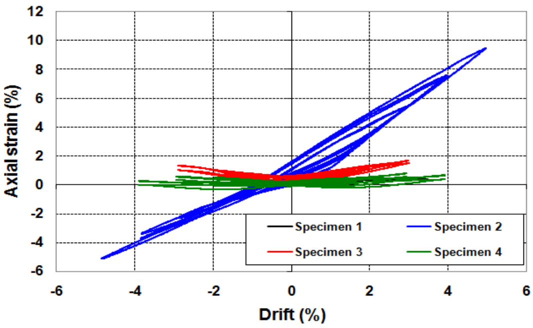

(b) Top

Fig. 28 Axial strain-West column

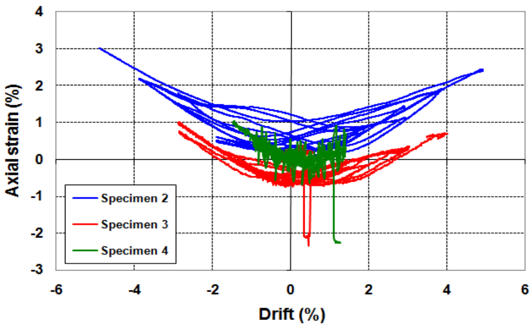

(a) Bottom

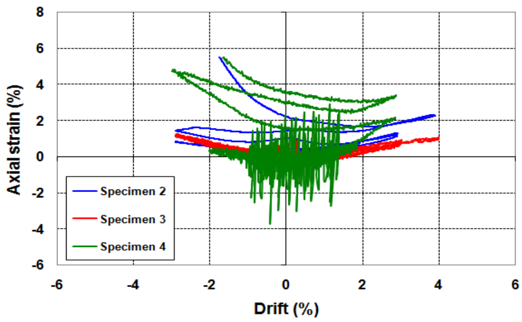

(b) Top

Fig. 29 Axial strain - East column

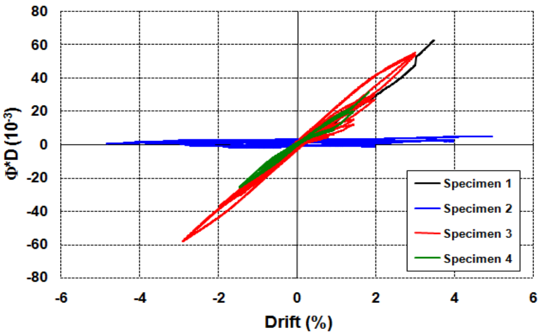

(a) Bottom

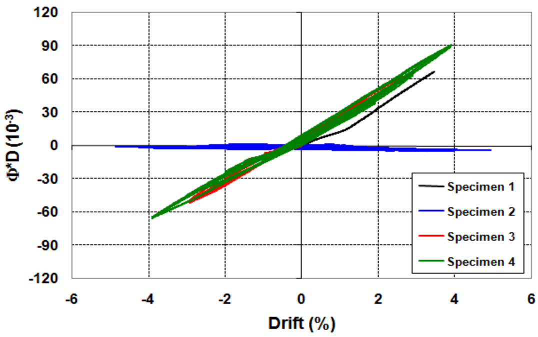

(b) Top

Fig. 30 Normalized curvature-drift relationships- West column

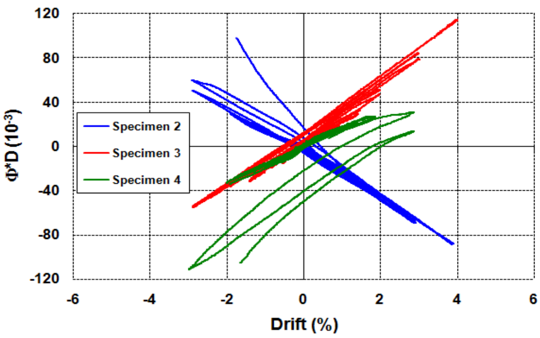

(a) Bottom

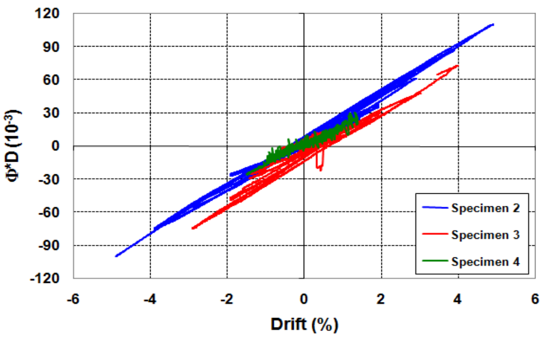

(b) Top

Fig. 31 Normalized curvature-drift relationships- East column

external hoops nor for the internal hoops. Table 9 shows the drift corresponding to the first yielding of the longitudinal reinforcements.

Table 10 Damage progress of specimen 1

Drift Range	Observed damage
R=1/500	Cracks appeared at 130 to 300 mm from the base of East column.
R=1/250	Cracks at 100 mm to 300 mm from the top of West column.
R=1/100	Several cracks appeared at the top of the two columns.
R=1/67	Opening between the top columns and the loading beam at the corner of the west and south sides.
R=1/50	Concrete spalling was observed at the top of the corners of the East column. The same damage was observed at the base of the West column.
R=1/33	A big openings were observed between the East and West columns and the foundation.

Table 11 Damage progress of specimen 2

Drift Range	Observed damage
R=1/500	First crack appeared at the first cycle from 100 mm to 200 mm from the columns bases.
R=1/250	At the first cycle, crack at 15 mm from the base of the West column appeared.
R=1/150	At the first cycle, crack appeared at 115 mm from the base of the East column.
R=1/67	Spalling of cover concrete at the corner base of the East and West columns.
R=1/33	Large openings (4 to 5 mm) were observed between the base of the columns and the foundation as well as between the top of the columns and the loading beam.
R=1/25	Buckling of the longitudinal reinforcement of East and West columns.
R=1/20	An important openings (10 mm) were observed between the base of the columns and the foundation as well as between the top of the columns and the loading beam.

Fig. 28 to Fig. 31 show a comparison between the four specimens in terms of the recorded axial strain and the normalized curvatures with respect to drift at the top and bottom parts (equal to the half of the column depth) of the west and east columns.

The axial strain is defined by the average displacement recorded by the two LVDTs divided by the height of the considered zone.

As illustrated in Fig. 28, the west column of specimen 2 demonstrated a large deformation (elongation and shortening) along the neutral axis of the column. The three other specimens show only elongation. While for the east column, only elongation was measured for specimens 2, 3 and 4, at the base and the top of the column, see Figs. 29(a)-(b). The west column of specimen 2, that showed an important values of the axial strain as discussed previously, showed this time a very small values of the normalize curvature compared to the three other specimens as seen in Figs. 30(a)-(b). Specimen 3 exhibited nearly the same values as specimen 4, see Figs. 30(a)-(b). Variation of the normalized curvature-drift relationships at the bottom of the east columns of specimen 2 and specimen 3 were close to each other as illustrated in Fig. 31(a).

(a) Specimen 1

(b) Specimen 2

Fig. 32 Damage pattern for bare frames

(a) Specimen 3,

(b) Specimen 4

Fig. 33 Damage pattern for frames with infill masonry panels

6.7 Failure modes

Crack propagation was monitored for all specimens since the apparition of the first crack, using the crack sale and by taking photos.

Table 10 to Table 13, summarize the damage progress for all specimens during the entire loading progress. As an example, Figs. 32-33 show, a state of the observed damage during the loading for bare frames and frames with infill masonry panels.

Table 12 Damage progress of specimen 3

Drift Range	Observed damage
R=1/500	A small opening was observed at the top corners of the masonry panel.
R=1/250	The first diagonal crack on the masonry panel appeared.
R=1/150	Appearance of the second diagonal crack on the masonry panel. An out off plane of 4 mm was measured between the panel and the West Column.
R=1/67	Damage to the top west corner of the masonry panel. Opening between the masonry panel, the two columns and the loading beam. Appearance of a hole at mid-height of the West part of the masonry panel.
R=1/50	Appearance of a hole at mid-height of the East part of the masonry panel. Damage to the upper parts of the two columns.
R=1/33	Increase of the size of the two holes in the masonry panel.

Table 13 Damage progress of specimen 4

Drift Range	Observed damage
R=1/500	Crack of the mortar clothing of the masonry panel at the angles of the opening.
R=1/250	At the first cycle, appearance of the first diagonal crack at the east upper corner of the masonry panel.
R=1/150	Cracks appeared at the base and the top of the East and West columns. Cracks of the masonry panel at the top west and east angle of the opening.
R=1/100	Cracks of the masonry panel at the west side of the opening. At the first cycle, damage of the mortar clothing at the upper part of masonry panel. Appearance of new cracks at the base and the top of the East and West columns
R=1/67	Sliding for 3 mm between the upper part and the lower part of masonry panel at the base of the opening.
R=1/50	Damage to the masonry panel at the west and the east sides of the opening.

6.8 Crack width

The crack width is an important index for evaluating the damage level of RC structure. Photos of the observed damage as well as the crack's widths were taken at different drifts and different locations. As an example; Fig. 34 shows the Crack widths measured at two different locations on the east column of specimen 1.

The value of the maximum crack was 1.2 mm for the east column. Locations of the monitored cracks are those shown in Fig. 35.

Fig. 36 illustrates the crack width variation for specimen 2 at different locations of the east and west columns, shown in Figs. 37(a)-(b). The value of the maximum crack was 0.8mm for the east column. For the west column, crack was

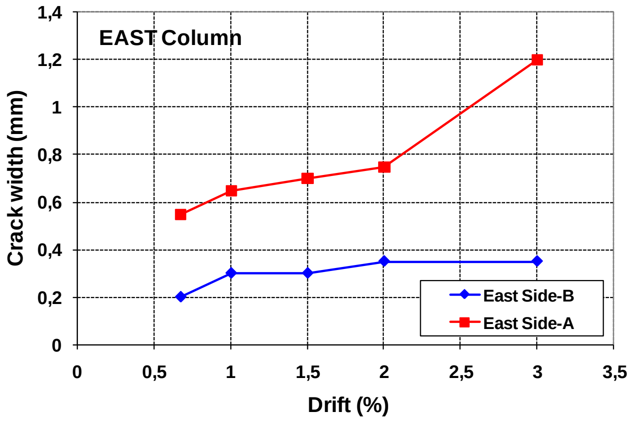

Fig. 34 Crack width evolution of specimen 1

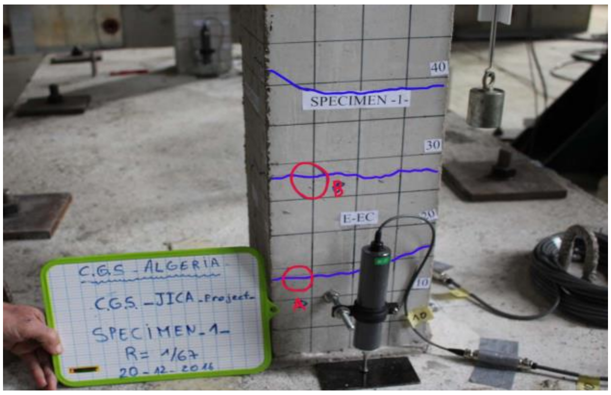

Fig. 35 Crack pattern of specimen 1, East column , East side at *R*=1/67

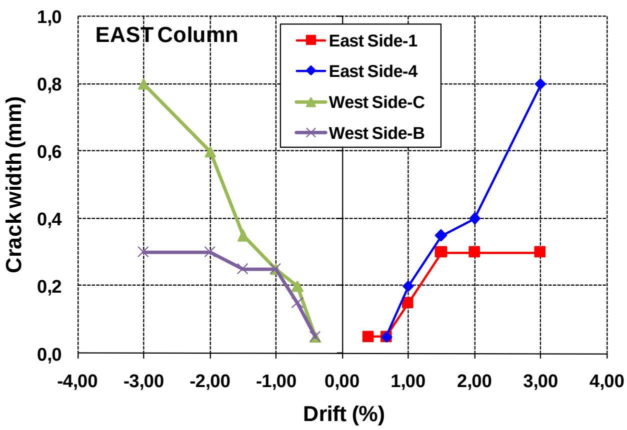

Fig. 36 Crack width evolution of specimen 2

more important at top part of the column than at the bottom part.

For specimens 1 and 2, damage was localized at the extremities of the columns for a height equal half of the column depth.

Fig. 38 illustrate the crack width variation for specimen 3 at different parts of the east and west columns. Location and label of the different cracks are also shown in Figs. 39(a)-(b). Value of the crack widths were nearly the same for the two columns, nearly 0.5 mm at the top of the column and 0.4 mm at the bottom.

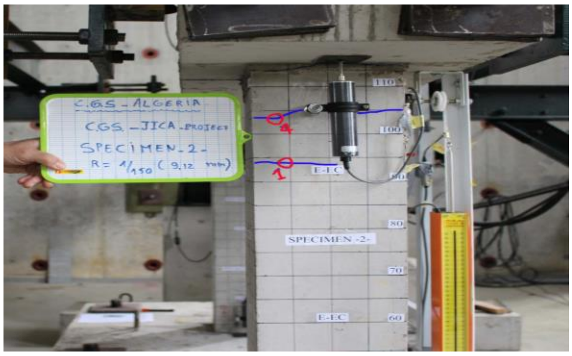

(a) East side 3

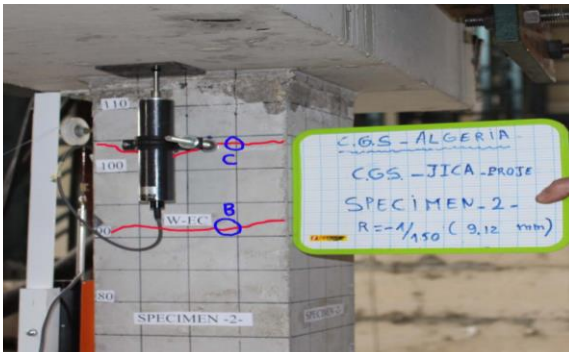

(b) West side

Fig. 37 Crack pattern of specimen 2, East Column, at *R*=1/150

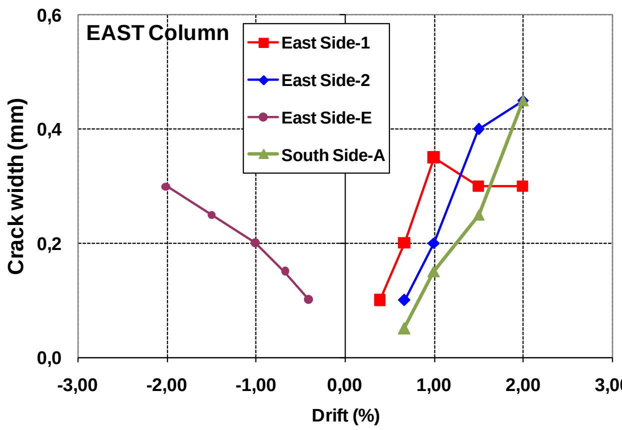

Fig. 38 Crack width evolution of specimen 3

Fig. 40 and Fig. 41 show the locations/labels and the crack width variations for the east column of specimen 4. The maximum crack width, 0.8mm, was measure on the south side of the east column.

7. Numerical simulation

Over the past few decades, several methods for the analysis of infilled frames have been proposed in the literature by various authors. These methods can be divided into two groups micro models and macro models (Sayed and Majid 2016).

In our case, numerical macro-models for the tested specimens were developed and analyzed using finite element SeismoStruct software (SeismoStruct 2016).

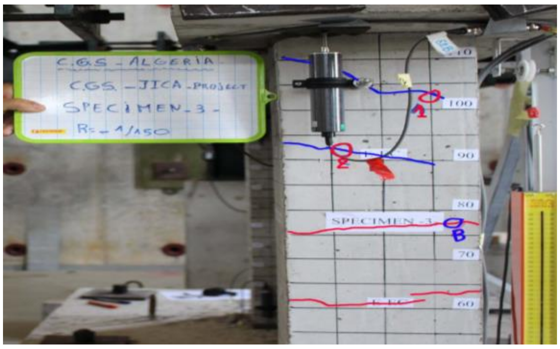

(a) East side

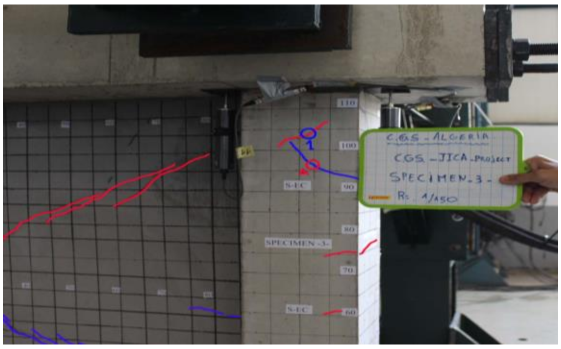

(b) South side

Fig. 39 Crack pattern of specimen 3, East column at *R*=1/150

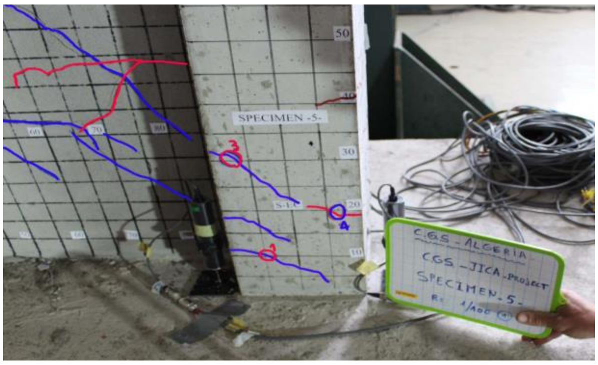

(a) South side

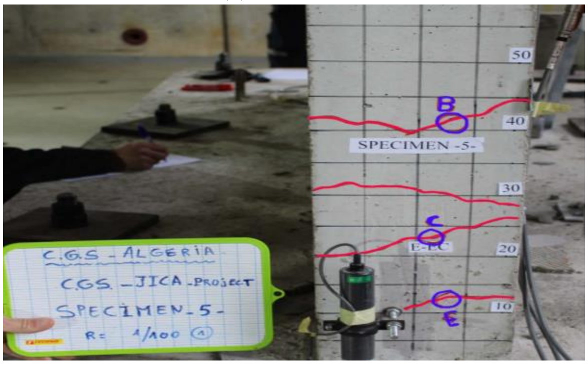

(b) East side

Fig. 40 Crack pattern of specimen 4, East column at *R*=1/100

The RC frame was modeled by an assemblage of inter-connected frame elements using distributed material inelasticity through displacement based formulation. Each

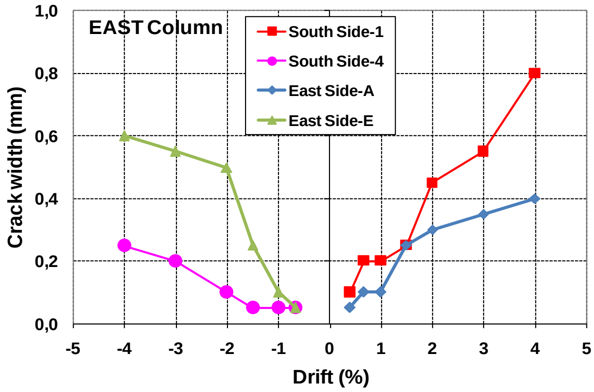

Fig. 41 Crack width evolution of specimen 4

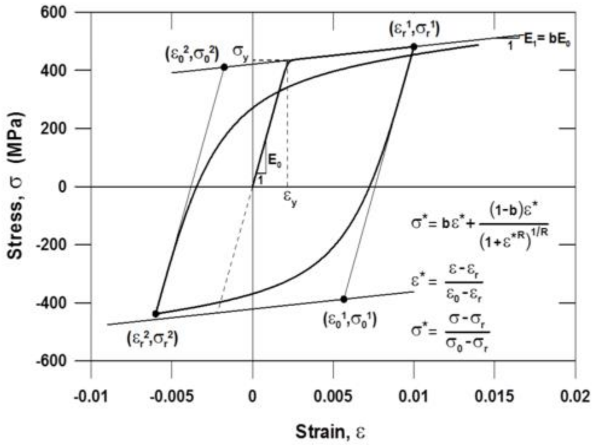

Fig. 42 Constitutive Model for steel (Menegotto and Pinto, 1973)

element was discretized into four sub-elements with two integration points each. Fiberized cross-sections were then defined at respective integration points. Every fiber was assigned to an appropriate material constitutive relationship.

To define the stress-strain behavior of concrete, Mander model was used while in case of steel reinforcement, Menegotto - Pinto model was used. Post-elastic and elastic stiffness ratio and the shape defining parameters are adjusted to conform the stress-strain behavior accurately in Menegotto-Pinto model, as shown in Fig. 42. The isotropic strain hardening effects is introduced and calibrated through inputs variables a_1 and a_2 for compression side and a_3 and a_4 for the traction side (Menegotto and Pinto 1973).

The nonlinear response of the masonry infill panels was modeled by using a plane stress infill panel element developed by Crisafulli and Carr (2007). The model is implemented as a four-node panel element which is connected to the frame at the beam-column joints. The infill panel is represented by six strut members in the equivalent strut model, as shown in Fig. 43.

Each diagonal direction features two parallel struts to carry axial loads across two opposite diagonal corners and a third one to carry the shear from the top to the bottom of the panel. This latter strut only acts across the diagonal that is under compression; hence its activation depends on the deformation of the panel (Shahriar *et al.* 2013). The nonlinear response of the axial and shear struts was

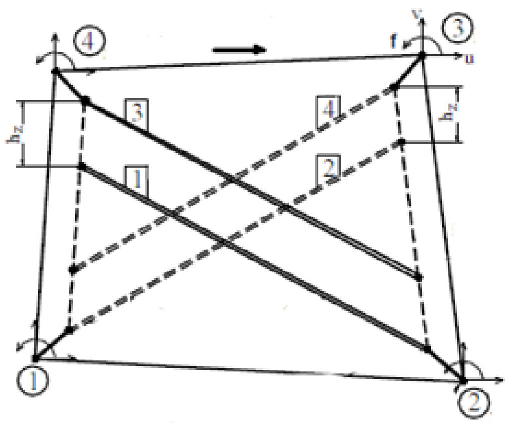

(a) Truss mechanism

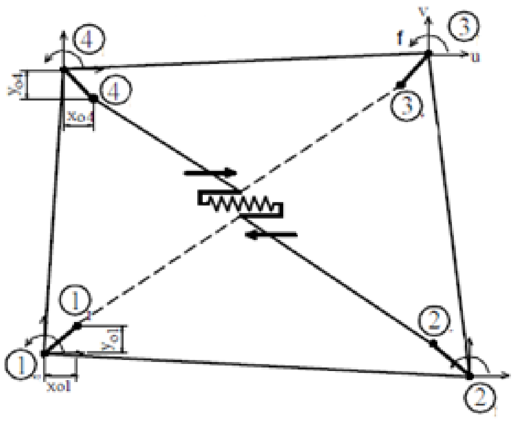

(b) Shear behavior

Fig. 43 Four-node masonry panel element (Crisafulli 2007)

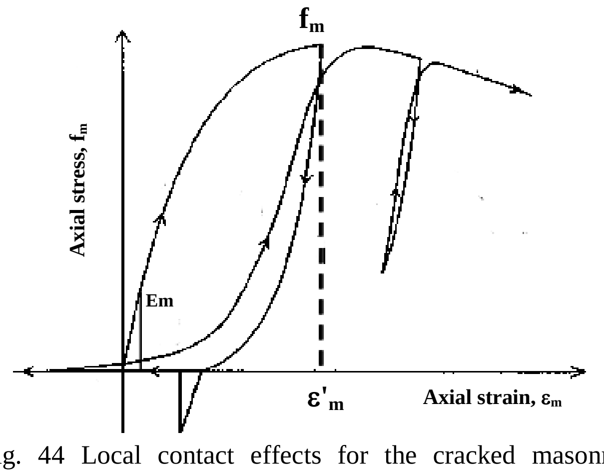

Fig. 44 Local contact effects for the cracked masonry (Crisafulli 1997)

modeled by adopting the hysteresis and bilinear model proposed by Crisafulli (1997).

Specific conditions were introduced by Crisafulli (1997) in the hysteresis model in order to simulate the contact effects which produce wider hysteresis loops and gradual increase of the compressive stress in the reloading process. An example of the cyclic response including contact effects is illustrated in Fig. 44. Analytical response for cyclic shear response of mortar joints is presented in Fig. 45.

The total strut member's stiffness is distributed in a

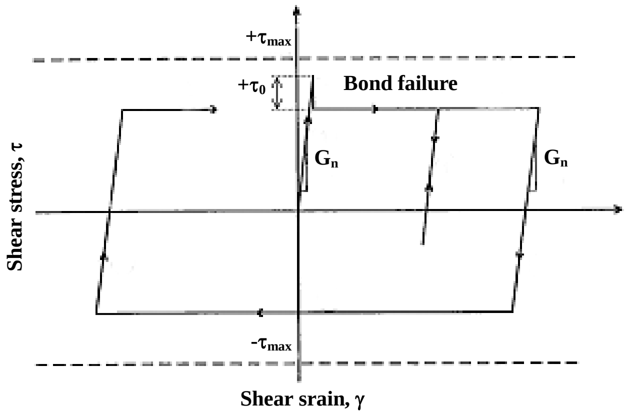

Fig. 45 Analytical response for cyclic shear response of mortar joints (Smyrou 2006)

given proportion to the shear spring k_s and to the struts k_A as given by the flowing equations (Crisafulli 1997)

$$K_s = \gamma_s \frac{A_{ms} E_m}{d_m} \cos^2 \theta \tag{8}$$

$$K_A = (1-\gamma_s) \frac{A_{ms} E_t}{2d_m} \tag{9}$$

Where γ_s is the percentage of total stiffness received by the shear spring, E_m is the elastic modulus of the masonry, E_t is the tangent modulus of the masonry defined according to an adequate hysteretic model for masonry, A_{ms} is the area of the struts, d_m and θ are the length and the inclination respectively of the diagonal of the panel. The area strut is defined as the product of the panel thickness and the equivalent width of the strut b_w. In the literature, numerous empirical expressions have been proposed by different authors for the evaluation of the diagonal width.

The area of the equivalent strut can decrease due to the reduction of the contact length between the panel and the frame, and due to the cracking of the masonry infill. It is assumed in the model that the area of the equivalent varies linearly as a function of the axial displacement.

The horizontal and vertical offset, x_{0i} and y_{0i} represent the reduction of the infill panel's dimensions due to the depth of the frame members.

The vertical separation h_z between struts leads to good results for values of 1/3 to 1/2 of the contact length.

Three different sets of nodes are considered for the development of the panel element, namely, external nodes, internal nodes and dummy nodes. The external nodes are those connected to the principal structure, whereas the internal nodes are defined by a horizontal and a vertical offset, x_{0i} and y_{0i} respectively.

Three degrees of freedom, the two translations and the rotation, are considered in each of the external and internal nodes. Four dummy nodes, with two translational degrees of freedom per node, are required to define the end of the strut members which is not connected to the corners of the panel.

In summary, the model consists of numerous parameters that can be classified in 1) mechanical (compressive

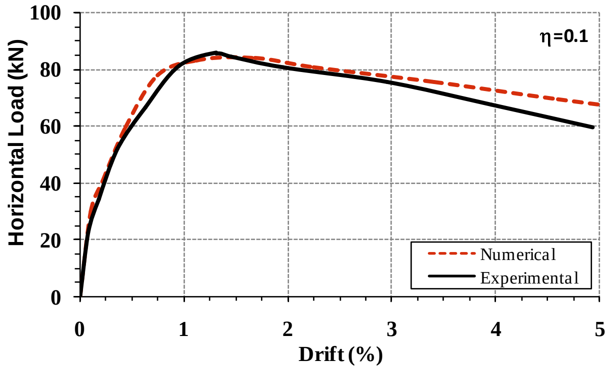

Fig. 46 Load-drift envelope curves-Bare Frame

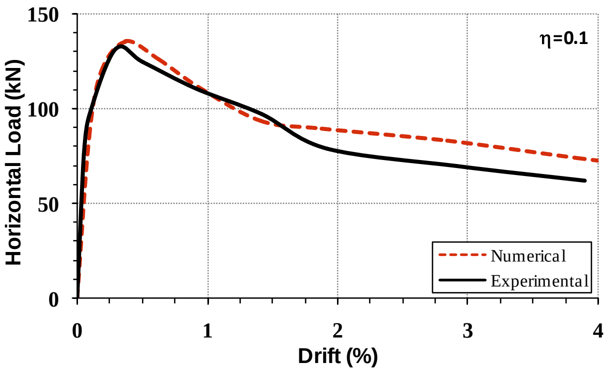

Fig. 47 Load-drift envelope curves-Full Panel

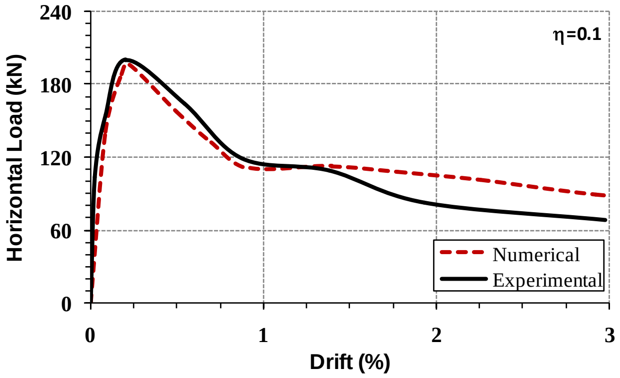

Fig. 48 Load-drift envelope curves-Panel with opening

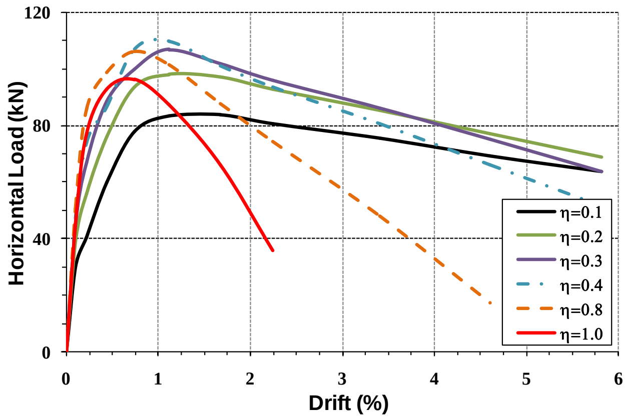

Fig. 49 Load-drift envelope curves for various axial loads Bare Frame

strength, elastic modulus, tensile strength, bond shear strength and strength), 2) geometrical (area of strut and vertical separation between struts) and 3) empirical parameters (eleven parameters were obtained after experimental results). More explanations about the meaning and the range of recommended values of the empirical parameters are given by Smyrou (2006).

In order to analyze the influence of the openings on the behavior of the infill masonry panel, several researchers have proposed many procedure in which the load path around the opening is simulated by the application of several struts capturing the force path around the opening or by adopting reduction factors for the geometrical properties of the strut which would be used in the case of infill panel without openings Smyrou (2006). The effect of masonry panel may be ignored if the area of opening exceeds 40% of the area of the infill panel and the frame will be analyzed as a bare frame (Goutam and Sudhir 2008). In our work, the effect of opening is taken into account by reducing the value of the Strut Area, and hence of the panel's stiffness in order to get the correct value of peak load and lateral stiffness.

The numerical models of the specimens tested were calibrated in order to match the envelope of hysteresis curves of the experimental tests.

The calibrated models are used in the parametric study to determine the envelope curve for various values of normalized axial loads.

The numerical results, obtained for normalized axial load equal to 0.1, in terms of the envelope curves for the tested specimens, bare frame, frame with full panel and frame with opened panel, were compared with experimental results in Fig. 46, Fig. 47 and Fig. 48, respectively.

As illustrated in the Figs. 46-47-48, the numerical results for all specimens show good agreement with the experimental ones. It can be seen that, the deviation in the estimation of the peak load value stated in about ±10% range of the experimental values.

In addition, initial stiffness value, for all specimens, was adequately estimated by the numerical model. However, some differences were found after the post-peak, descending branches of the load-drift envelope curve, corresponding to 3% drift for specimen 2 and 1.5% drift for specimen 3 and 4. It was observed that, beyond these limits, the deviation between the numerical and the experimental results becomes around 15% for RC bare frame and 25% for frames with infill panels.

Parametric study, based on the FE model described before, was carried out to analyze the effect of axial load intensity η on the horizontal load-drift relationships of the tested specimens. Figs. 49-50-51 shows the comparison of the lateral force versus story drift relations of RC bare frame, frame with full panel and frame with opened panel obtained for various normalized axial loads, η.

It can be seen from Fig. 49, that the peak load increase with increase in the normalized axial load, when the value of normalized axial load is about 0.8 the peak load start to reduce. However, an abrupt decay is detected in the post peak portions of the load drift envelope obtained for values

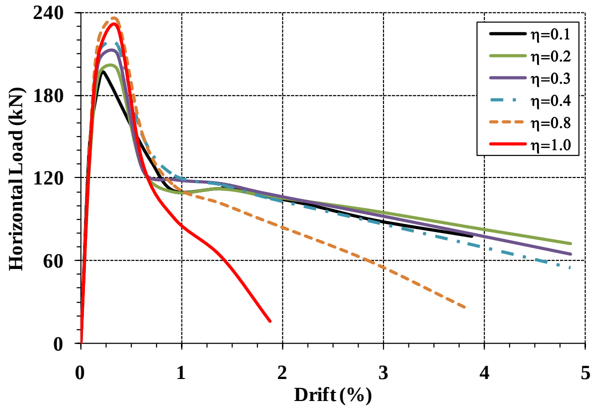

Fig. 50 Load-drift envelope curves for various axial loads Frame with Full Panel

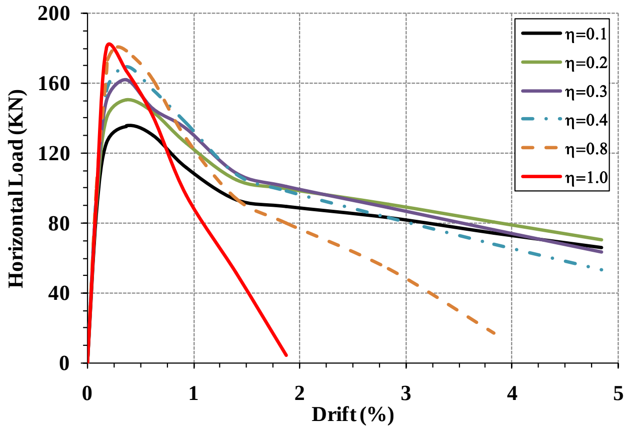

Fig. 51 Load-drift envelope curves for various axial loads Frame with opened Panel

of normalized axial load over 0.4.

From Figs. 50-51, the same effect of axial load intensity was observed while comparing the envelope curves of the infilled frames, frame with full panel and frame with opened panel.

Fig. 52 shows a comparison between the considered models in terms of peak loads ratio. The peak load ratio is defined as the peak load obtained for various normalized axial load to the peak reached for the same model for 0.1 of the normalized axial load value. It is seen from Fig. 48 that the peak load ratio increases almost linearly with increase of normalized axial load for all models. A descending branch was observed on the post peak load ratio at normalized axial load of 0.4 for bare frame and 0.8 for infilled models.

In addition, the variation of the peak load ratio of bare frame is significantly higher compared to frame with full panel and frame with opened panel.

A comparison between the peaks obtained for the infilled models and bare frame model are shown in Table 14. For frame with full masonry infill panel model, the peak load ratios varied between 2 to 2.4 times, while compared to the peaks load reached for the bare frame for the same value of normalized axial load. These values were, respectively, 1.5 and 1.8 for frame with an centric opening infill masonry panel.

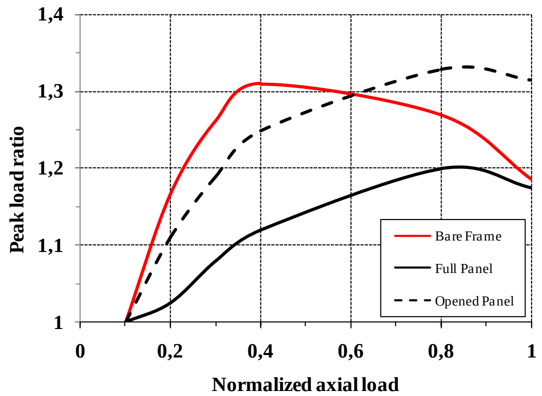

Fig. 52 Variation of peak load ratio

Table 14 Specimen's peak to bare frame peak ratios

Normalized axial load	0.1	0.2	0.3	0.4	0.8	1.0
Frame with full panel	2.4	2.10	2.05	2.04	2.26	2.37
Frame with opened panel	1.63	1.55	1.54	1.55	1.71	1.81

For a RC frame building design, the Algerian seismic code, RPA99/2003 (MHUV 2003), limit the value of normalized axial load to 0.3 for columns.

8. Conclusion

The object of this research was to investigate experimentally the seismic behavior of RC frames infilled with masonry under constant vertical and reversed cyclic lateral loads. Four specimens of one storey, one bay frames with two types of masonry configuration (“full panel” and “panel with opening”) infill panel were tested and their response was compared with that of bare frames.

The specimens were a half-scale (1/2) models taken from a real building constructed before the last version of the Algerian seismic code RPA99/2003. The test results showed that at low levels of lateral displacements, the composite frame- masonry acted monolithically as one element. The masonry infill, due to its high stiffness, stiffened the bare frame and also increased its initial strength. As the cracks developed in the masonry, the masonry infill panel partially detached from the surrounding frame. Behavior of RC frame depends on the type of separation and the length of the remaining contact zone between the masonry infill and frame. Once the masonry was severely damaged, the columns became the last line of resistance of the frames.

The mains results of this experimental investigation can be summarized as follow:

• Infill panel have a large effect on the behavior of frames under cyclic loading. In general, infill panels contributed to the stiffness and strength of the structure.

• Specimen with infill panel (with and without opening) was much brittle while bare frame specimen exhibit larger ductility.

• Sway mechanism was observed during the test due to the so called cold joint between the foundation and the bottom of the column and the top column and the loading beam, which let the flexural contribution to the top displacement very small compared to that of shear contribution.

• For the bare frames (specimens 1 and 2), damage was localized at the extremities of the columns for a height equal half of the column depth.

• Yielding of the longitudinal reinforcements was observed for the four specimens. However, transversal reinforcement did not yield.

• Masonry infill panel (with and without opening) increased the height of the bottom cracked zone of column and made the column crack at a earlier stage.

• For specimen with a full masonry panel, diagonal cracks firstly appeared at the center of the wall, which propagated to the corners in the subsequent loading cycles. For the opened infilled frame, the opening acted as crack initiator with cracks propagating from its corner.

• Stiffness degradation of the bare frame (specimen 2) is less pronounced than that observed for the frame with infill masonry (specimens 3) and the frame with opened masonry (specimen 4).

• Infilled frame exhibited a better energy dissipation capacity, especially for the fully infilled frames.

• As for the equivalent viscous damping, H_{eq}, it was observed that beyond 2% drift for specimen 3 and 3% drift for specimen 4, the two specimens showed nearly the same slope on the H_{eq}-drift curves as the bare frame, specimen 2.

Numerical macro-models for the tested specimens were developed using the finite element SeismoStruct software and calibrated with the experimental results. The numerical results for all specimens show good agreement with the experimental ones within an error of ±10%.

Investigation on the effect of axial load intensity on the horizontal load-drift relationships of the tested specimens was carried out. It was concluded that the application of vertical load higher to 0.4 of the normalized axial load, caused an effect on the seismic behavior of the bare frame. Other results of this investigation can be summarized as follow:

• Variation of the peak load ratio (defined as the peak load obtained for various normalized axial load to the peak reached for the same model for 0.1 of the normalized axial load value) of the bare frame is significantly higher compared to the frame with full panel and the frame with opened panel.

• For frame with full masonry infill panel model, the peak load ratios varied between 2 to 2.4 times, while compared to the peaks load reached for the bare frame for the same value of normalized axial load. These values were, respectively, 1.5 and 1.8 for frame with a centric opening infill masonry panel.

Based on the experimental and the numerical results we recommend that:

• The construction mode that is applied nowadays in Algeria, construction of the vertical element (columns and walls) after that construction of the floor, should be changed. The best way to avoid the cold joint is to construct a monolithic floor, by constructing the vertical elements and the floor at the same time.

• The Algerian seismic codes require revision to incorporate the effect of the masonry panel in the analysis and the design process related to such buildings, especially for moderate seismic zones.

Acknowledgments

The research described in this paper was financially supported by the National Earthquake Engineering Research Centre, CGS, Algeria and carried out with the technical cooperation of the Japan International Cooperation Agency, JICA, Japan.

References

Aksel, F., Baris, B., Pourang, E., Erdem, C. and Guney, O. (2016), "The effect of infill walls on the seismic behavior of boundary columns in RC frames", *Earthq. Struct.*, **10**(3), 539-562.

Alessandro, V.B. and Camillo, N. (2015), "Experimental tests and global modeling of masonry infilled frames", *Earthq. Struct.*, **9**(2), 281-303.

Ali, M., Behnam, M. and Mohammad, R.A. (2015), "Seismic response of RC frame structures strengthened by reinforced masonry infill panels", *Earthq. Struct.*, **8**(6), 1435-1452.

Bechtoula, H. (2002), "Damage assessment of reinforced concrete columns under large axial and lateral loadings", Master Degree, Kyoto, University, Japan.

Brokken, S. and Bertero, V.V. (1981), "Studies on effects of infills in seismic resistant RC construction", Report UCB/EERC, 81-12, University of California, Berkeley.

Calvi, G.M. and Bolognini, D. (2001), "Seismic response of reinforced concrete frames infilled with masonry panels weakly reinforced", *J. Earthq. Eng.*, **5**, 153-185.

Crisafulli, F.J. (1997) "Seismic behavior of reinforced concrete structures with masonry infills", PhD Thesis, Department of Civil Engineering University of Canterbury Christchurch, New Zealand, July.

Crisafulli, F.J. and Carr, A.J. (2007), "Proposed macro-model for the analysis of infilled frame structures", *Bull. NZ Soc. Earthq. Eng.*, **40**(2), 69-77.

Egermann, R., Cook, D.A. and Anzani, A. (1991), "An investigation into the behaviour of scale model brick walls", *Proceedings of the 9th International Brick/Block Masonry Conference*, Berlin, Germany.

Fabio, C. (2015), "Seismic behaviour of reinforced concrete frames with different configuration of masonry infill", Degree of Master Philosophy in Civil Engineering, University of Science and Technology, Hong Kong.

Flanagan, R.D. and Bennett, R.M. (1999), "In-plane behaviour of structural clay tile infilled frames", *J. Struct. Eng.*, ASCE, **125**(6), 590-599.

Ghassan, A. (2002), "Evaluating Strength and Stiffness of Unreinforced Masonry Infill Structures", US Army of Corps Engineers, ERDC/CERL TR-02-1.

Goutam, M. and Solomon, T. (2014), "Effects of vertical irregularity and thickness of unreinforced masonry infill on the robustness of RC framed buildings", *Earthq. Eng. Struct. Dyn.*, **43**(2), 205-223.

Goutam, M. and Sudhir, K.J. (2008), "Lateral stiffness of masonry infilled reinforced concrete frames with central opening", *Earthq. Spectra*, **24**(3), 701-723.

Hamid, R.K. and Kadir, M. (2016), "Experimental study of masonry infill reinforced concrete frames with and without corner openings", *Struct. Eng. Mech.*, **57**(4), 641-656.

Hanhui, Z., Kuang, J.S. and Terry, Y.P. (2017), "Low-seismic damage strategies for infilled RC frames: shake-table tests" *Earthq. Eng. Struct. Dyn.*, **46**(14), 2419-2438.

Hughes, T.G. and Kitching, N. (2000), "Small scale testing of masonry", *12th International Brick/Block Masonry Conference*, Madrid, Spain.

Ivan, R., Damir, M. and Vladimir, S. (2016), "Controlled seismic behavior of masonry-infilled steel frames", *Građevinar*, DOI: 10.14256/JCE.1673.2016, 11/2016.

Jarun, S., Sutat, L., Arnon, W. and Panitan, L. (2017), "Experimental and analytical evaluation of a low-cost seismic retrofitting method for masonry-infilled non-ductile RC frames", *Earthq. Struct.*, **12**(6), 699-712.

Kakaletsis, D. and Karayannis, C. (2007) "Experimental investigation of infilled r/c frames with eccentric openings", *Struct. Eng. Mech.*, **26**(3), 231-250.

Lotfi, H.R. and Shing, P.B. (1994), "An interface model applied to fracture of masonry structures", *J. Struct. Eng.*, ASCE, **120**(1), 63-80.

Maidiawati (2013), "Modeling of brick masonry infill for seismic performance evaluation of RC frame buildings", Doctor of Engineering, Toyohashi University of Technology.

Masanori, H. and Kheir-Eddine, R. (2004), "Boumerdes Earthquake the 21st May 2003", Japanese Reconnaissance Team, technical Report, DOI: 10.13140/RG.2.2.36186.34249.

Menegotto, M. and Pinto, P.E. (1973), "Method of analysis of cyclically loaded RC plane frames including changes in geometry and non-elastic behavior of elements under normal force and bending", *Proceedings of IABSE Symposium on Resistance and Ultimate Deformability of Structures Acted on by Well Defined Repeated Loads*, 15-22.

Ministère de l'Habitat et de l'Urbanisme, M.H.U.V. et Centre National de Recherche Appliquée en Génie Parasismique, C.G.S. (2003), Règlement Parasismique Algérien, RPA 99 version 2003, Algeria.

Ministère de l'Habitat et de l'Urbanisme, M.H.U.V. et Centre National d'Etudes et de Recherches Intégrées du Bâtiment, CNERIB (2005), "Règles de conception et de calcul des maçonneries DTR C2-45", Algeria.

Misir, I.S., Ozcelik, O., Sadik, C.G. and Serap, K. (2012), "Experimental work on seismic behavior of various types of masonry infilled RC frames", *Struct. Eng. Mech.*, **44**(6), 763-774.

Ousalem, H. and Bechtoula, H. (2003), "Report on the damage investigation and post-seismic campaign of the 2003 Zemmouri Earthquake in Algeria", The University of Tokyo Department of Architecture 2003 by Earthquake Research Institute, The University of Tokyo C/O Kabeyasawa Laboratory, Division of Disaster Mitigation Science, Tokyo, Japan.

Ozakaynak, H., Yuksel, E., Yakin, C., Dindar, A.A. and Buyukozturk, O. (2015), "Masonry infill walls in reinforced concrete frames as a source of structural damping", *Earthq. Eng. Struct. Dyn.*, **43**(7), 949-968.

Pinto, A.V., Varum, H. and Molina, J. (2000), "Experimental assessment and retrofit of full-scale models of existing RC frames", *Proc. 12th ECEE*, London.

Preti, M., Bettini, N. and Plizzari, G. (2012), "Infill walls with sliding joints to limit infill-Frame seismic interaction: large-scale experimental test", *J. Earthq. Eng.*, **16**(1), 125-141.

Sayed, M.M.E. and Majid, M. (2016), "Influence of vertical load on in-plane behavior of masonry infilled steel frames", *Earthq. Struct.*, **11**(4), 609-627.

SeismoSoft (2016), SeismoStruct-A Computer Program for the Static and Dynamic Analysis of Framed Structures, http://www.seismosoft.com.

Shabdin, M., Attari, N.K. and Zargaran, M. (2018), "Experimental study on seismic behavior of Un-Reinforced masonry (URM) brick walls strengthened with shotcrete", *Bull. Earthq. Eng.*, **16**(9), 3931-3956.

Shabita, A. and Sozen, M.A. (1976), "Substitute structure method for seismic design in RC", *J. Struct. Div.*, ASCE, **102**(ST1), 1-18.

Shahriar, Q., Shahria, M.A. and Rteil, A. (2013) "Seismic behavior of soft storey mid-rise steel frames with randomly distributed masonry infill", *Steel Compos. Struct.*, **14**(6), 523-545.

Smyrou, L. (2006), "Implementation and verification of masonry panel model for nonlinear dynamic analysis of infilled RC frame", PhD in European School for Advanced Studies in Reduction of Seismic Risk, Rose school, Pavia, Italy.

Stylianidis, K.C. (2012), "Experimental investigation of masonry infilled R/C frames", *Open Constr. Build. Technol. J.*, **6**, 194-212.

Teguh, M. (2017), "Experimental evaluation of masonry infill walls of RC frame building subjected to cyclic loads", *Procedia Engineering*, SCESCM, Sustainable Civil Engineering Structures and Construction Materials.

Terry, Y.P.Y., Han-hui, Z., Kuang, J.S. and Qunxian, H. (2018), "Shake table tests on RC frame infilled by slitted masonry panels", *Bull. Earthq. Eng.*, **16**(9), 4027-4052.

Tsung-Chih, C. and Shyh-Jian, H. (2015), "Tests on cyclic behavior of reinforced concrete frames with brick infill" *Earthq. Eng. Struct. Dyn.*, **44**(12), 1939-1958.

Yasushi, S., Yoshiaki, N., Kazuto, M., Devjyoti, P., Polat, G. and Baris, B. (2017), "Experimental evaluation of the in-plane behaviour of masonry wall infilled RC frames", *Bull. Earthq. Eng.*, **15**(10), 4245-4267.

CC